Investigating the physical properties of outbursts on comet 67P/Churyumov–Gerasimenko

Zhong-Yi Lin, Jörg Knollenberg, Jean-Baptiste Vincent, Michael F. A'hearn, Wing-Huen Ip, Holger Sierks, Cesare Barbieri, Philippe Lamy, Rafael Rodrigo, Detlief Koschny, et al.

Monthly Notices
of the
ROYAL ASTRONOMICAL SOCIETY
MNRAS **469,** S731–S740 (2017) doi:10.1093/mnras/stx2768

Investigating the physical properties of outbursts on comet 67P/Churyumov–Gerasimenko

Zhong-Yi Lin,[1★] J. Knollenberg,[2] J.-B. Vincent,[2] M. F. A'Hearn,[3] W-H. Ip,[1,4,5] H. Sierks,[6] C. Barbieri,[7,8] P. L. Lamy,[9] R. Rodrigo,[10,11] D. Koschny,[12] H. Rickman,[13] H. U. Keller,[14] S. Mottola,[2] D. Bodewits,[3] J. Agarwal,[6] M. A. Barucci,[15] J.-L. Bertaux,[16] I. Bertini,[7] G. Cremonese,[17] J. Deller,[6] V. Da Deppo,[18] B. Davidsson,[19] S. Debei,[20] M. De Cecco,[21] S. Fornasier,[15] M. Fulle,[22] O. Groussin,[9] P. J. Gutiérrez,[23] C. Güttler,[6] M. Hofmann,[6] S. F. Hviid,[2] L. Jorda,[9] G. Kovacs,[6] J.-R. Kramm,[6] E. Kührt,[2] M. Küppers,[10] I.-L. Lai,[5] L. M. Lara,[23] M. Lazzarin,[8] J-C. Lee,[24] J. J. López-Moreno,[23] F. Marzari,[7] G. Naletto,[25] N. Oklay,[2] T. Ott,[26] E. Drolshagen,[26] X. Shi,[6] N. Thomas[27] and C. Tubiana[6]

Affiliations are listed at the end of the paper

Accepted 2017 October 19. Received 2017 October 19; in original form 2017 April 10

ABSTRACT

Cometary outbursts on several comets have been observed both by ground-based telescopes and by *in situ* instruments on spacecraft. However, the mechanism behind these phenomena and their physical properties are still unclear. The optical, spectrocopic and infrared remote imaging system (OSIRIS) onboard the *Rosetta* spacecraft provided first-hand information on the outbursts from comet 67P/Churyumov–Gerasimenko during its perihelion passage in 2015. The physical properties of the outbursts can be investigated by examining the time series of these high-resolution images. An analysis is made of the wide- and narrow-angle images obtained during the monitoring of the outburst sequences, which occurred between July and September in 2015. A ring-masking technique is used to calculate the excess brightness of the outbursts. The ejected mass and expansion velocity of the outbursts is estimated from differences in images made with the same filter (orange filter). The calculated excess brightness from these outburst plumes ranges from a few per cent to 28 per cent. In some major outbursts, the brightness contribution from the outburst plume can be one or two times higher than that of the typical coma jet activities. The strongest event was the perihelion outburst detected just a few hours before perihelion. The mass ejection rate during a generic outburst could reach a few per cent of the steady-state value of the dust coma. Transient events are detected by studying the brightness slope of the outburst plume with continuous streams of outflowing gas and dust triggered by driving mechanisms, as yet not understood, which remain active for several minutes to less than a few hours.

Key words: comets: individual: 67P/Churyumov–Gerasimenko.

1 INTRODUCTION

The optical, spectrocopic and infrared remote imaging system (OSIRIS) scientific imaging cameras on the *Rosetta* spacecraft have been monitoring the coma activity of comet 67P Churyumov–Gerasimenko (67P hereafter) since their orbital rendezvous in 2014 August (Lara et al. 2015; Lin et al. 2015; Sierks et al. 2015; Lin et al. 2016; Shi et al. 2016; Vincent et al. 2016a,b). The solar heating of the sunlit side of the nucleus surface leads to sublimation of the volatiles and to the formation of dust jets. On 2015 March 12, a small outburst was first detected from a part of the Imhotep region on the night side (Knollenberg et al. 2016). Such mini-outbursts or night-side activities have been observed before at comet 9P/Tempel

★ E-mail: zylin@astro.ncu.edu.tw

1 by the *Deep Impact* mission (Farnham et al. 2007, 2013) and comet 103P/Hartley 2 by the *EPOXI* mission (A'Hearn et al. 2011; Bruck Syal et al. 2013). Shortly before the close approach to comet 9P/Tempel 1, the high-resolution camera on the *Deep Impact* spacecraft found a number of small, well-defined jets whose bases were rooted at the nucleus surface. Some of these, called limb jets, appeared to come from the darker regions and appeared to be associated with the ice patches reported by Sunshine et al. (2006). A later mission of the *Stardust*–New Exploration of comet Tempel 1 (NExT) imaging of 9P/Tempel 1 allowed us to connect the jets with cliffs (Farnham et al. 2013). Comet 103P/Hartley 2 also displayed several narrow jet features emitting from the un-illuminated regions beyond the terminator at the time of the flyby observations (Bruck Syal et al. 2013). Unlike the less certain identification of the source regions on Tempel 1, the source region of the nightside jets of 103P/Hartley 2 could be clearly traced to some rough surface topography. However, the mechanism for this type of activity is still unknown. Fortunately, unlike the snap shots from the previous flyby observations, the OSIRIS measurements can provide precise information on the timing and location of the outbursts via a time series of high-resolution images. After the first detection in 2015 March, the OSIRIS wide-angle camera (WAC) and narrow-angle camera (NAC) captured another outburst in mid-July of 2015. Since then, many more outbursts from the nightside and sunlit regions have been detected (Feldman et al. 2016; Grün et al. 2016), with most of their source regions located in the Southern hemisphere of comet 67P (Vincent et al. 2016a). The detected outburst events show a variety of morphological features that can be classified into three different types: broad fans, narrow jets and complex plumes. In this work, we investigate the morphology of these events and characterize their physical properties in detail, including the surface brightness profiles, ejected mass and speed if there are two or more sequential images acquired by the same filter in short duration during the time frame of the outburst.

2 OBSERVATIONS AND DATA ANALYSIS

The data sets used in the present investigation consist of pairs of consecutive images obtained within a short time interval of ∼6 s to ∼20 s in the period 2015 July 29 to September 30 (∼ one month before and after the peak of the water production rate; Hansen et al. 2016), with an NAC orange filter (centre wavelength = 6486 Å, FWHM = 852.4 Å). The observational data for all images listed in Table 1 were acquired in 1 × 1 binning mode, which results in a pixel scale of ∼3 to ∼26 m, depending on the changing distances between the *Rosetta* spacecraft and the nucleus. Fig. 1 shows that an example of an outburst event can be easily detected without any image enhancement technique or highlighting of the image using a specific display scale (i.e. log–log scale).

Fig. 2 shows an example of a case where additional image processing must be applied to find the outburst events directly from the consecutive images. These low-contrast mini-outbursts can be extracted through image differencing as the activity becomes stronger or weaker with time. In this work, we used the positive detection method to obtain the physical properties of the outbursts from difference images.

Several data sets from both the NAC and WAC were especially designated for monitoring the activity of the nucleus. The observed sequences ranged from 1 h to one full rotation (∼12.4 h). Starting in late August in 2015, sequences of high-cadence observations (every 5 min) in some sequences were designed to search for outburst events. Before then, normal cadences of 20 or 30 min for the NAC and 1 h for WAC had been scheduled. The observation log is summarized in Table 1.

3 RESULTS

3.1 Brightness variation

The excess brightness contributed by the outburst plumes can, in principle, be estimated directly from the images in the corresponding sequences. The computational steps are as follows: the comet nucleus is blocked out from the centre to a certain cut radius depending on how large the nucleus is; the excess brightness within a specified narrow 'ring' region can be estimated by counting the pixels where the jet-like features are enhanced by an azimuthally averaged background division measurement (Lin et al. 2015). Assuming that the background coma is distributed uniformly in the azimuthal direction, the excess brightness can be attributed to the jet-like features. Note that the jet-like features can be classified into those emerging from the illuminated regions, called coma jets, and the new-born jet-like features arising from the transient events (outbursts), called the outburst plume. If we account for the viewing geometry in the outburst sequences and follow the assumption that the outburst event is responsible for any increase in the transient coma brightness, the variations in brightness can be determined. Several cases are discussed below. Fig. 3(a) shows the brightness variation of the strongest outburst detected on 2015 August 12. This event is also called the perihelion outburst because it occurred just a few hours before the comet reached perihelion. The scheduled sequence, spanning almost 15.3 h (∼1.25 full rotation), was ideal for monitoring the activity. However, it is not easy to estimate how much of the excess brightness comes from the outburst plume because the contribution from the jet-like features from different illuminated regions is hard to evaluate. Coincidentally, the sequence taken in the last few hours has a similar viewing geometry and the coma jet activity within these hours does not show large variations, showing about 20 per cent before and after the perihelion outburst. As a result, the maximum additional excess brightness of the perihelion outburst on 17.34 UT can be estimated to be close to 30 per cent higher than that contributed from the coma jet activity.

The outburst sequences, as the name suggests, were carried out to search for outbursts within a short duration (∼1 to 1.25 h). Given the condition of a similar viewing geometry, the excess brightness of an outburst detected on 2015 September 3 is about 7.4 per cent more than the total brightness of the coma jets, which is about ∼22 per cent, as shown in Fig. 3(b). The calculated excess brightness of the outburst plumes observed in the period 2015 July to September could range from a few per cent to a few dozen per cent.

According to Lin et al. (2015), the excess brightness from the coma jet activities in 2014 when comet 67P was at the heliocentric distance of 3.53–3.29 au was 3–10 per cent. When comet 67P moved closer to its perihelion in 2015 August, the excess brightness from the coma jet activities increased to 10–25 per cent of the uniform coma at a heliocentric distance of 1.24–1.38 au. Our results are consistent with the results from onboard instruments (for MIRO and GIADA), which indicated that comet 67P showed higher levels of activity in the weeks around perihelion as a result of intense solar radiation that caused the gas and dust to stream into space at an ever greater rate.

Table 1. Observational log of the images that have outbursts. SC distance is the distance between the spacecraft and the centre of comet 67P. The phase angle is the Sun–comet–observer (OSIRIS) angle. Type denotes the morphological classification of the outburst plumes defined by Vincent et al. (2016a).

Start time (UT)	r_h (au)	SC distance (km)	Pixel scales (m pixel^{-1})	Phase angle (degree)	Type	Slope (k) (fitting range, in m)
Difference images (NAC orange filter)						
2015-07-29 13:24:10.760	1.2561033	186.299	3.42	89.8849	A	0.304 (200–4400)
2015-08-05 07:10:32.077	1.2469707	253.369	4.67	89.5959	B	1.247 (50–1500)
2015-08-05 08:03:57.736	1.2469355	253.263	4.67	896098	B	2.123 (500–2000)
2015-08-12 17:20:36.436	1.2432693	331.920	6.13	89.4620	C	0.643 (300–2000)
2015-08-16 22:53:06.769	1.2441791	329.730	6.09	89.2077	B	1.575 (300–2000)
2015-08-26 08:19:55.322	1.2539818	417.171	7.72	83.6198	A	0.638 (400–2000)
2015-08-27 03:12:06.804	1.2552807	403.175	7.46	79.7127	A	0.840 (100–1000)
2015-08-28 10:09:51.784	1.2575693	410.290	7.59	73.5676	B	1.916 (200–2000)
2015-09-03 17:57:22.781	1.2715593	379.504	7.02	86.7103	C	1.089 (50–300)
2015-09-03 18:02:22.782	1.2715682	379.577	7.02	86.7482	C	1.089 (100–1000)
2015-09-03 18:07:22.801	1.2715772	379.651	7.02	86.7859	C	1.157 (100–1500)
2015-09-03 18:12:22.782	1.2715861	379.726	7.02	86.8237	C	1.209 (100–1100)
2015-09-03 18:17:22.812	1.2715950	379.802	7.02	86.8614	C	0.817 (200–1100)
2015-09-03 18:22:22.799	1.2716039	379.879	7.02	86.8991	C	1.166 (100–650)
2015-09-03 18:27:22.764	1.2716129	379.955	7.03	86.9367	C	0.828 (100–400)
2015-09-03 18:32:22.856	1.2716218	380.035	7.03	86.9744	C	0.958 (100–400)
2015-09-03 18:37:22.857	1.2716307	380.113	7.03	87.0123	C	1.004 (100–400)
2015-09-03 18:42:22.814	1.2716396	380.193	7.03	87.0499	C	1.021 (100–400)
2015-09-03 18:47:22.797	1.2716486	380.273	7.03	87.0875	C	0.933 (50–300)
2015-09-03 18:51:32.792	1.2716560	380.341	7.03	87.1188	C	1.234 (50–400)
2015-09-03 18:22:22.799	1.2716039	379.879	7.02	86.8991	B	1.556 (500–6000)
2015-09-05 08:23:55.782	1.2758057	437.494	8.10	99.9797	A	0.594 (200–2000)
2015-09-05 08:58:43.857	1.2758816	435.401	8.06	100.0881	C	0.505 (300–8000)
2015-09-08 22:40:38.846	1.2863748	336.620	6.22	118.2778	A	0.945 (200–2000)
2015-09-10 20:51:22.797	1.2925862	317.807	5.87	119.9952	A	1.063 (100–2000)
2015-09-10 21:11:12.538	1.2926324	317.873	5.87	119.9904	A	1.336 (400–3000)
2015-09-12 09:41:53.733	1.2978142	329.892	6.09	116.5622	C	1.180 (1000–4500)
2015-09-12 09:46:53.760	1.2978263	329.819	6.09	116.5383	C	1.008 (1000–4500)
2015-09-12 09:51:53.715	1.2978384	329.746	6.09	116.5146	C	1.030 (1000–4500)
2015-09-12 09:56:53.734	1.2978505	329.673	6.09	116.4907	B	1.112 (1000–4500)
2015-09-23 21:59:37.739	1.3442340	402.277	7.44	71.8011	B	3.528 (200–600)
2015-09-24 22:56:47.769	1.3490112	545.744	10.11	59.6096	B	2.205 (160–500)
2015-09-24 23:31:46.762	1.3491240	549.625	10.18	59.4261	A	1.063 (100–2000)
2015-09-25 04:18:13.134	1.3500487	581.974	10.78	58.0488	C	1.519 (1000–4500)
2015-09-25 05:48:13.288	1.3503399	592.337	10.98	57.6587	A	0.982 (200–4500)
2015-09-25 09:09:39.809	1.3509930	615.833	11.41	56.8516	B	1.826 (100–1000)
2015-09-25 09:14:38.751	1.3510091	616.419	11.42	56.8326	C	0.531 (600–3000)
2015-09-25 09:54:38.764	1.3511390	621.134	11.51	56.6830	A	1.001 (200–1000)
2015-09-25 10:39:39.757	1.3512852	626.457	11.61	56.5184	A	0.931 (100–500)
2015-09-25 10:54:38.831	1.3513339	628.232	11.64	56.4644	A	1.791 (200–2000)
2015-09-30 11:36:45.774	1.3758860	1456.540	27.05	50.2459	A	0.661 (200–2000)
2015-09-30 21:34:37.765	1.3780003	1399.900	26.00	50.4653	B	1.913 (200–2000)
2015-09-30 23:29:55.513	1.3783900	1389.010	25.79	50.5092	A	0.847 (200–2000)
Sequences used for estimating the brightness variations						
2015-08-12 (WAC, UV375)	1.24330 to	338.898 to	34.00 to	89.7335 to		
07.01 20.20	1.24326	329.475	33.05	89.3681		
2015-08-22 08-23 (WAC, UV375)	1.24916 to	333.872 to	133.96 to	88.5106 to		
21.46 02.11	1.24938	334.503	134.24	88.2005		
2015-09-03 (WAC, UV375)	1.27152 to	379.214 to	76.14 to	86.5581 to		
17.37 18.51	1.27166	380.338	76.38	87.1176		
2015-09-12 (NAC, ORANGE)	1.29969 to	320.395 to	5.92 to	112.76830 to		
22.30 23.25	1.29982	319.853	5.91	112.487		

3.2 Brightness profiles

Another important OSIRIS result is comprised of the radial brightness profiles, which can be used to understand the physical properties and to derive the outflow speed of the dust particles in the outburst plumes. The brightness distributions of the coma jets and outburst plumes arising in the outbursts along the radial distance is determined by taking the relation of $B \sim \rho^{-k}$, where B is the coma jet and outburst plume brightness, ρ is the projected distance from the comet centre perpendicular to the camera–comet centre direction and k is the slope of the $\log B$ versus $\log \rho$ function (see Lin et al. 2015). One way to estimate the brightness slope is to subtract the mean background brightness of the faint coma

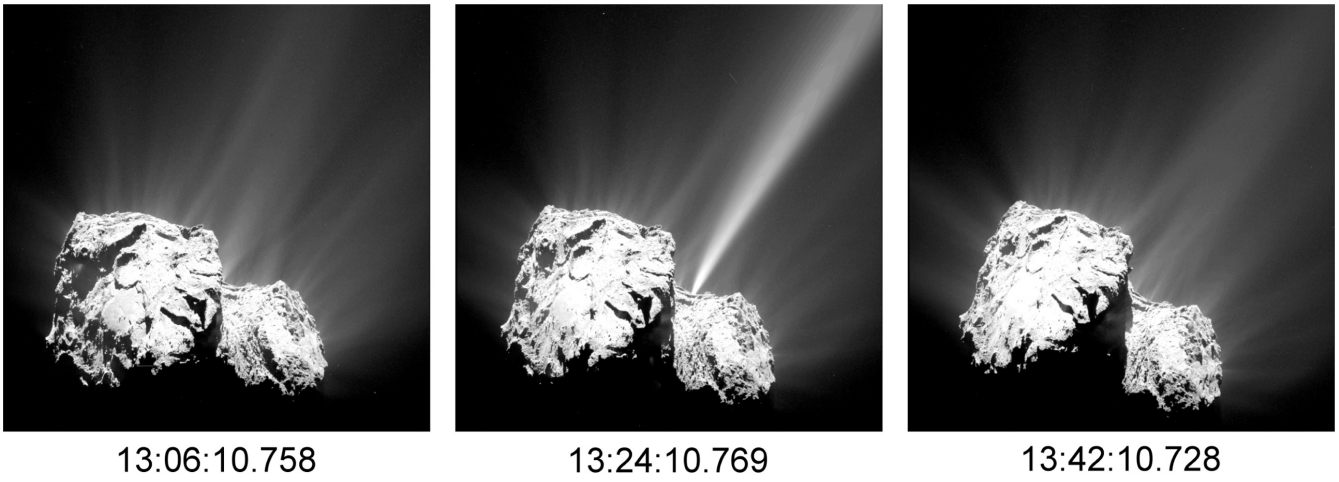

Figure 1. Time sequence of the coma structure on 2015 July 29 showing the sudden appearance of a dramatic outburst at 13:24 UT. The field of view (FOV) is $7 \times 7\,\mathrm{km}^2$. The Sun is coming from the top of the image.

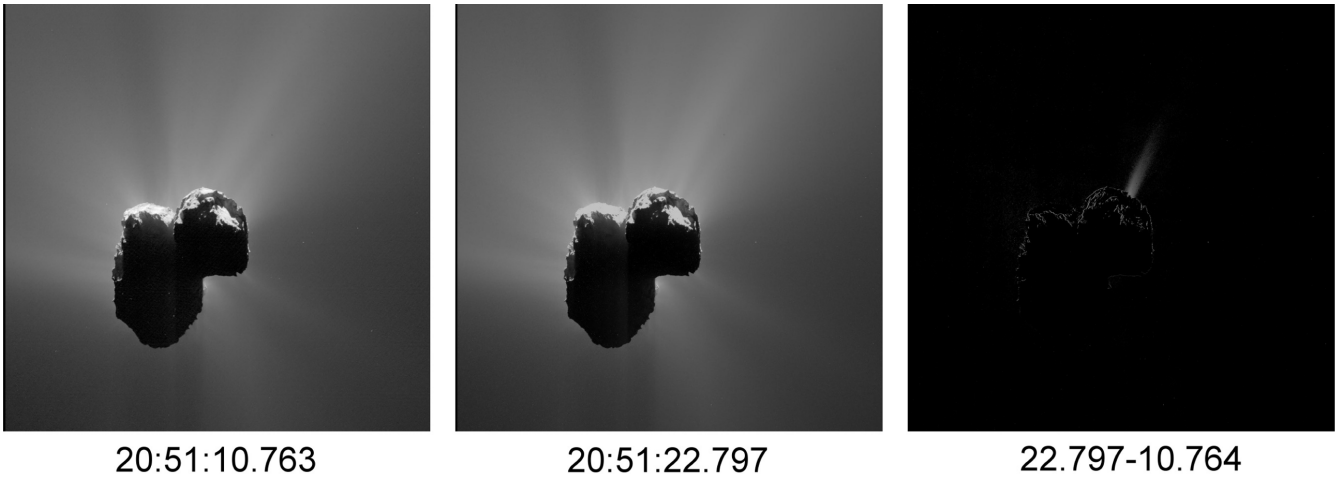

Figure 2. An example of how the difference image (right panel, 2015 September 10) obtained by subtracting the brightness of two images with a time interval of 12 s can extract an outburst feature when there is no clear detection from the consecutive images. The frame is $12.02 \times 12.02\,\mathrm{km}^2$. The Sun is towards the top.

surrounding the nucleus. This approach benefits from the observational condition (i.e. the fact that the *Rosetta* spacecraft was relatively far away from the nucleus during the perihelion passage so that a large portion of the background coma was in view). This means that the nucleus is relatively small and we can compute the low contamination values of the coma background directly from the image. Fig. 4 shows an example of a slope measurement from the outburst image. Another way to obtain the brightness slope of the outburst plume is to determine it directly from the difference image (e.g. Fig. 2). Note that the slopes are extracted from the outburst plumes using the averaged profile within the selected box (see Fig. 6, for example), and from the coma jets using a central line along the radial direction of the coma jet (Fig. 4). We find that the slopes of the outburst plumes (see Table 1) vary between shallower than -1 and steeper than -2, depending on the morphology of the outburst plume. The type B (broad plume) slope is much steeper than that in the type A (collimated plume) slope. Although the brightness slopes vary over a wide range, they all follow the rule that the steeper slopes indicate an outburst plume and the flatter slopes indicate the background coma. The slopes of the coma jets fall in between. The respective slopes in between might refer to the different physical properties (i.e. grain size distributions) in the inner coma. Further detailed modelling of the overall slopes is therefore absolutely necessary.

Additionally, the radial brightness profile measured along the outburst plume can be used to derive the outflow speed of the dust if a reference image with a similar viewing geometry has been acquired before the outburst (Knollenberg et al. 2016). This can be illustrated by a simple model (Knollenberg et al. 2016). Fig. 5(a) shows the radiance on the jet axis for one particular size of the ejection dust particle (i.e. 223 μm in radius) as a function of time after the outburst starts (at $t = 0$). The progress of the leading edge is evident, which can be used to estimate the dust speed, whereas the inner part close to the nucleus approaches a steady state, meaning the production rate is constant. The associated difference images results (see Fig. 5b) show the leading edge as a kind of shell travelling outside, the position of which can be used to estimate the actual position of the leading edge. Although the shell feature is not found in the difference image, the local minimum outflow speed can be derived from the leading edge of the outburst plume. Fig. 6

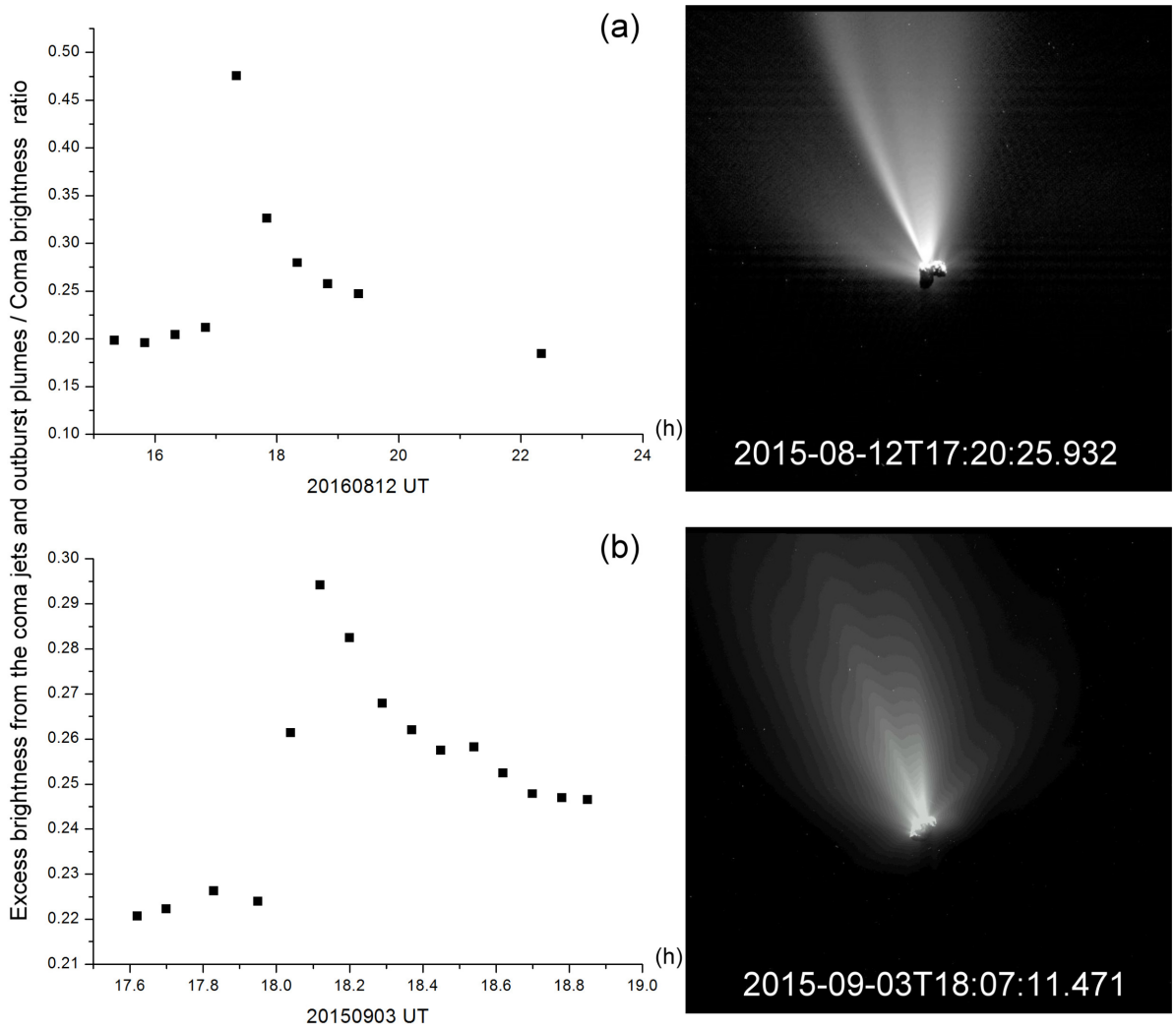

Figure 3. The coma brightness variation estimated from two different sequences: the activity monitoring sequence (top-left panel) and the outburst sequences (bottom-left panel) from the filter UV375 in the WAC. The related outburst images detected at the time of peak value in coma brightness ratio are shown in the right panels. The FOV of these two WAC frames is 67.78 km (a) and 177.65 km (b) and the Sun is towards the top. The maximum excess brightness for the outburst plume is derived from the comparison in between the base that mostly came from the contribution of the coma jets and the peak of the brightness variation.

shows one of these computable data sets and its corresponding radial brightness profile. The subtracted background level, indicated by the horizontal dashed line in Fig. 6 is about 3.2–3.4 $\times$ 10^{-7} (W m^{-2} nm^{-1} sr^{-1}). The vertical dotted line ($\sim$3000 m) indicates how far the dust particles have travelled within the time interval (12.03 s) within the difference image. Because of the projected effect, the lower limit of the dust ejection velocity for 2015 September 10 can therefore be determined ($\sim$243 m s^{-1}).

We found that the observed projected velocities of outburst plumes range from several tens of m s^{-1} to a few hundred m s^{-1} with no differences between the type of outbursts. Moreover, we do not find any shell structure along the outburst plume, reflecting that this is a complicated process or that there is a change in physical properties during the outburst. One possibility would be a broad size distribution instead of a single size as assumed in Fig. 5. In this case, the larger grains would move more slowly so it would take a longer time (perhaps longer than the duration of the outbursts) for a steady state to be established close to the nucleus. The absence of the shell structure could also mean that the production from the outburst source is increasing over the considered time interval instead of being constant. Alternatively, the dust size distribution within the outburst plume changes as a function of time along the outburst plume or energy is released by different outburst mechanisms. A changing size distribution would mean that the outburst plume might contain some icy particles that could affect the velocities when they are sublimating and fragmenting (Ipatov & A'Hearn 2011). The icy grains would be more highly reflective than dust particles and thus could dominate the measured velocities. So far, however, there is no evidence to support the fact that such sublimating icy grains exist around the nucleus of comet 67P (Schulz et al. 2015; Gicquel et al. 2016). In other words, the outburst mechanisms play an important role when measuring the expansion velocity.

3.3 Mass of the ejected material

In the calculation of the mass content of the particles required to produce an outburst of a certain brightness, particles 1 μm and larger should be the main contributors to the visual coma brightness. In reality, we will have a size distribution with smaller particles more

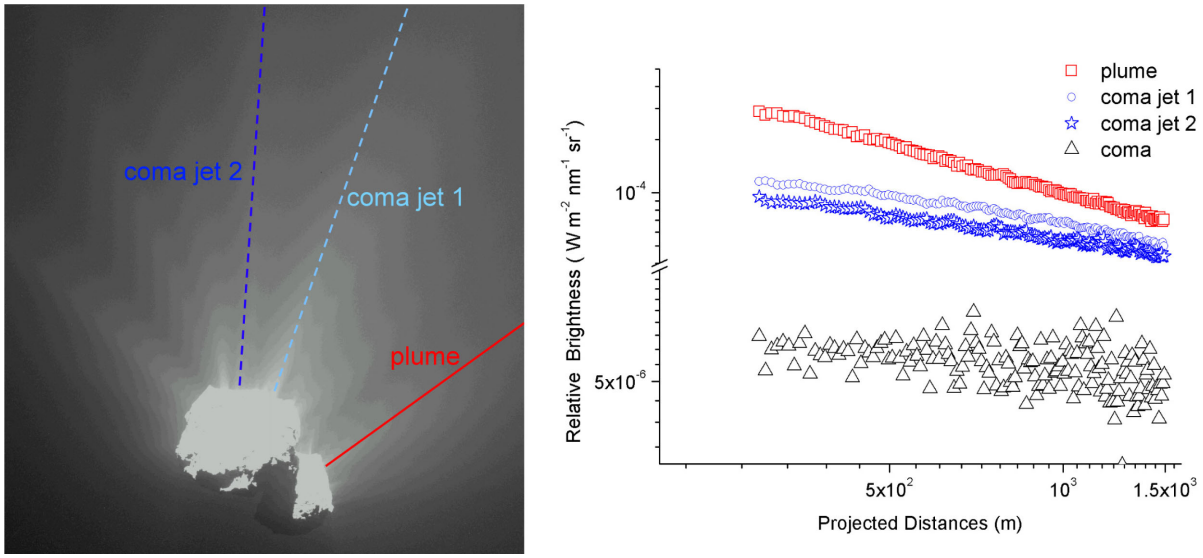

Figure 4. The brightness slopes with log–log scale (right panel) were measured including the outburst plume/ejecta (red square), coma jets (blue circle and star) and background coma (black triangle) from the OSIRIS individual image (left panel) obtained on 2015 September 23 from a distance of 402 km using the NAC with the orange filter. The frame is 20.85 × 20.85 km^2. Note that all the measured profiles are subtracted by the background coma.

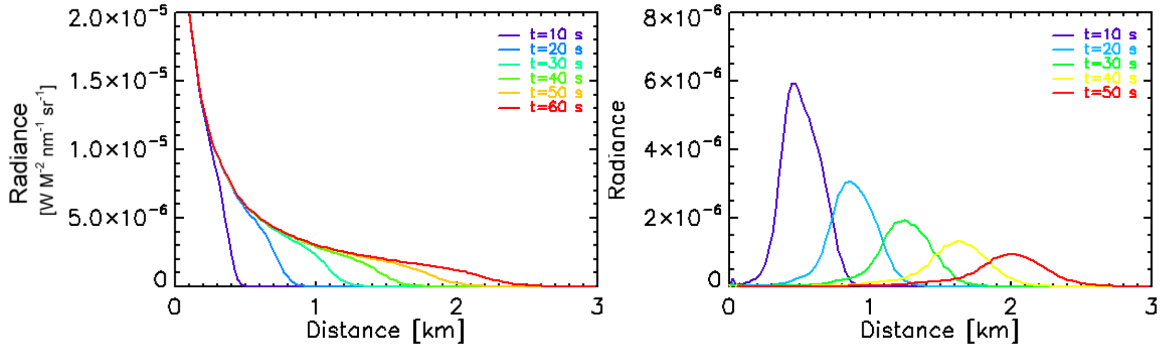

Figure 5. Assuming a constant production rate, outflow speed and one particular size of dust particle (i.e. 223 μm in radius), the simulated radiance along the outburst plume as a function of time is shown in the left panel. After subtracting the reference image taken before the outburst started, the leading edge as a shell moving outward is shown in the right panel.

abundant than larger particles, meaning that the largest particles will contain most of the ejected mass. The size distribution in the investigation is $n(r_d) \sim r_d^{-g}$ and the results show a significant change in the size distribution of the grains from the early phase in late 2014 to the perihelion in 2015. For instance, according toes Fulle et al. (2015) and Rotundi et al. (2015), the size distribution cannot be fitted by a single power-law model, as the heliocentric distance of comet 67P is larger than 3 au. Instead, they infer a knee-like size distribution with a corner radius of 0.5 mm and a differential size distribution exponent of $g = 4$ for large particles and an exponent ~ 2 for smaller particles. Knollenberg et al. (2016) investigated an outburst from the night-side part of the Imhotep region at the heliocentric distance of 2.2 au in 2015 March, and found that the outburst plume possibly consists mostly of small particles (<1 mm) following a power-law size distribution with $g = 2.6$. Fulle et al. (2016) claimed further that $g \sim 3.7$ for small particles ($a < 1$ mm) and 4.0 for large particles ($a > 1$ mm) at perihelion (~1.2 au). We note that the modelling results of the size distribution for the 2016 March outburst are compatible with the analysis of Fulle et al. (2016) for the same period of time. Therefore, we assumed a constant power-law index of $g = 3.7$ and a wide particle size range (from μm to mm) when calculating the mass of the dust ejected in the outburst. In addition to the size distribution, we need to estimate the cross-section of the dust particles. The method for estimating the dust cross-section from the difference images is described below and can also be found in Knollenberg (2016).

The specific radiance received from the optically thin dust plume can be expressed as

$$L_\lambda = f_{\rm plume} \frac{p}{\pi} \frac{\phi(\alpha)}{\phi(0)} \frac{f_\lambda}{{r_h}^2} \quad (1)$$

where p is the geometric albedo of the dust particles at wavelength λ, $\phi(\alpha)$ is the phase function at phase angle α, f_λ is the solar irradiance (in W m^{-2} nm^{-1} at 1 au), r_h is the heliocentric distance in au and $f_{\rm plume}$ is the dust filling factor (e.g. the fraction of a pixel covered by dust). Assuming that the geometric albedo of the dust particles is similar to that of the nucleus, the geometric albedo and specific solar flux are 0.068 and 1.513 W $^{-2}$ nm^{-1} for the orange (648.6 nm) filter, and 0.027 and 0.23 W $^{-2}$ nm^{-1} for the UV (270.7nm) filter (Fornasier et al. 2015), respectively. The flux ratio $\phi(\alpha)/\phi(0)$ can be derived by using the dust phase function (Kolokolova & Kimura 2010). By integrating the radiance over the image area (e.g. within the boxes in Fig. 7) containing the dust from a difference outburst plume, the total cross-section from difference images of

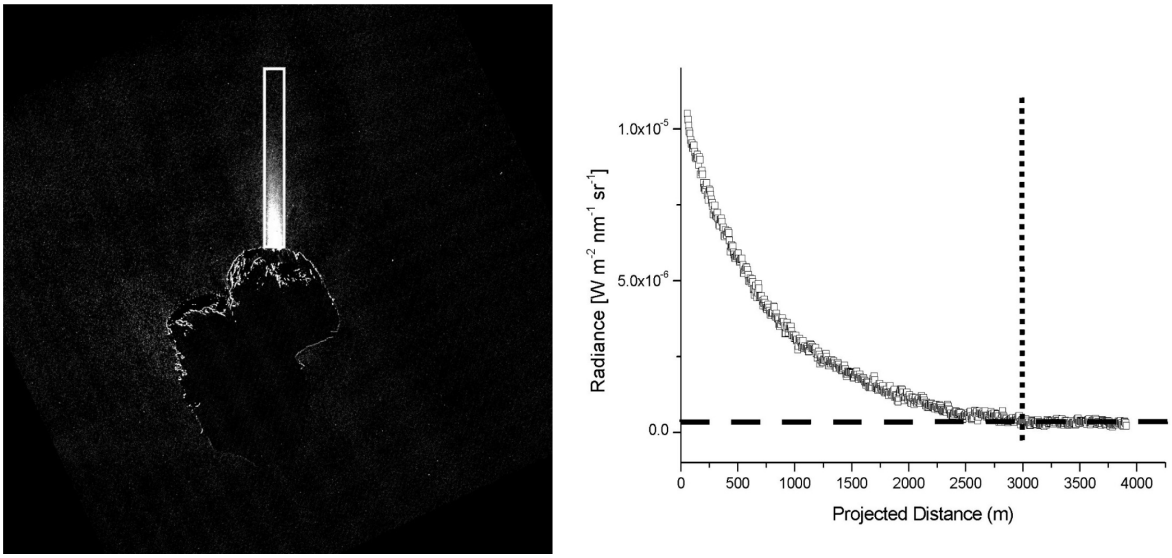

Figure 6. An example of how the leading edge determined from the difference image on 2015 September 10 (20:51:22.797) is used to derive the expansion velocity (left panel). A radial brightness profile (right panel) is an averaged value outwards from the nucleus in the selected box marked in the difference image. The subtracted background level is shown by the dashed line. The cross match in between the radial brightness profile and subtracted background level is shown by the vertical dotted line.

the dust jet from within a given time interval can be determined. Then, we used a power-law index $g = 3.7$ for the size distribution with a constant bulk density of 1000 kg m^{-3} for all ejected particles. The ejected mass in size interval of $a_1 < a < a_2$ (i.e. 1 μm to 1 mm) is given by

$$M = \frac{(4/3)\pi\rho N}{4-g}\left(a_2^{4-g} - a_1^{4-g}\right), \quad (2)$$

where N is the total number of dust particles in the size interval 1 μm to 1 mm. The estimated dust cross-section and ejected mass are given in Table 2. The uncertainty of the ejected mass is typically of the order of 5–10 per cent, depending on the uncertainty on the brightness integration of the selected box. The averaged mass ejection rate for the outbursts can be estimated from the ejected mass (M) by dividing by the time interval between the difference images. Note that our calculation is based on the chosen time intervals and hence produces lower limits on the mass ejection rates. For example, the estimation of the ejected mass for a major outbursts on July 29 is about 4550 kg. Given a time interval of 18 min, the average mass ejection rate would be of the order of 4 kg s^{-1}. However, if this outburst lasted for a time interval of 5 min only, which is the cadence for the outburst sequence, the corresponding mass ejection rate would be as much as 15 kg s^{-1}.

Thus, if we take these sudden and short-lived outbursts into account, the average mass ejection rate from those consecutive images with a longer time interval might be an order of magnitude larger than our estimation. In comparison, the peak dust production rate of the coma near perihelion has been estimated to be 1500 kg s^{-1} (Fulle et al. 2016). Our derivation above shows that the mass ejection rate (Table 2) during a large outburst could reach a few per cent of the dust coma at most.

4 DISCUSSION

With increased heating by the Sun, the comet experiences a higher level of outgassing activity during the perihelion approach. The Microwave Instrument for the *Rosetta* Orbiter (MIRO) indicated that about 300 liters of water (10^{28} molecule) were ejected every second, meaning that the comet was losing 26 million kg of water per day during this period (Fougere et al. 2016). Another 260–390 million kg of dust per day were lost when the dust-to-water mass ratio was around 10 at perihelion, as estimated by Fulle et al. (2016). The activity remained high for several weeks after perihelion, making it more difficult to obtain the excess brightness and the brightness slopes for the outburst plumes. The jet activities also exhibited diurnal variation with the rotation of the nucleus. If we assume that there was no significant change in repeatable coma jets emanating from the sunlit side during several full rotational periods, we can derive accurate values for the excess brightness and the brightness slopes by analysing images taken with different viewing geometries.

Furthermore, we note that the variability of the brightness profiles indicates that the outburst plumes, coma jets and background coma are not, in fact, in a steady state. In the pre-landing phase at around 3.5–3.3 au in 2014, we found steeper slopes (0.95–1.48) caused by the acceleration of the dust from the coma jets. In comparison, the slopes found for coma jets around the perihelion are not consistent with those in the pre-landing phase, indicating the existence of less volatile grains or different physical properties (i.e. size distributions). The outburst plumes also vary over a wide range depending on their morphology. Some do not seem to be extreme cases (steeper or shallower slopes). One possible explanation is that at least the overwhelming majority of cometary outbursts in the detected images are not explosions but rather continuous streams of outflowing gas and dust triggered by an outburst mechanism that has not yet been fully understood, which then remain active for some minutes to less than a few hours. Additionally, we found that some of the increasing average mass ejection events could last for a few tens of minutes (less than a half hour) while some are seen only in pairs of consecutive images. This could be explained by an inadequate fuel supply or by mechanisms that we do not fully understand. In a previous study, a strong increases in the rate of crystallization was proposed as a possible cause of the mini-outbursts observed in comet Tempel 1, during the intensive campaign in 2005 (Smoluchowski 1981; Prialnik, Bar-Nun & Podolak 1987; Prialnik,

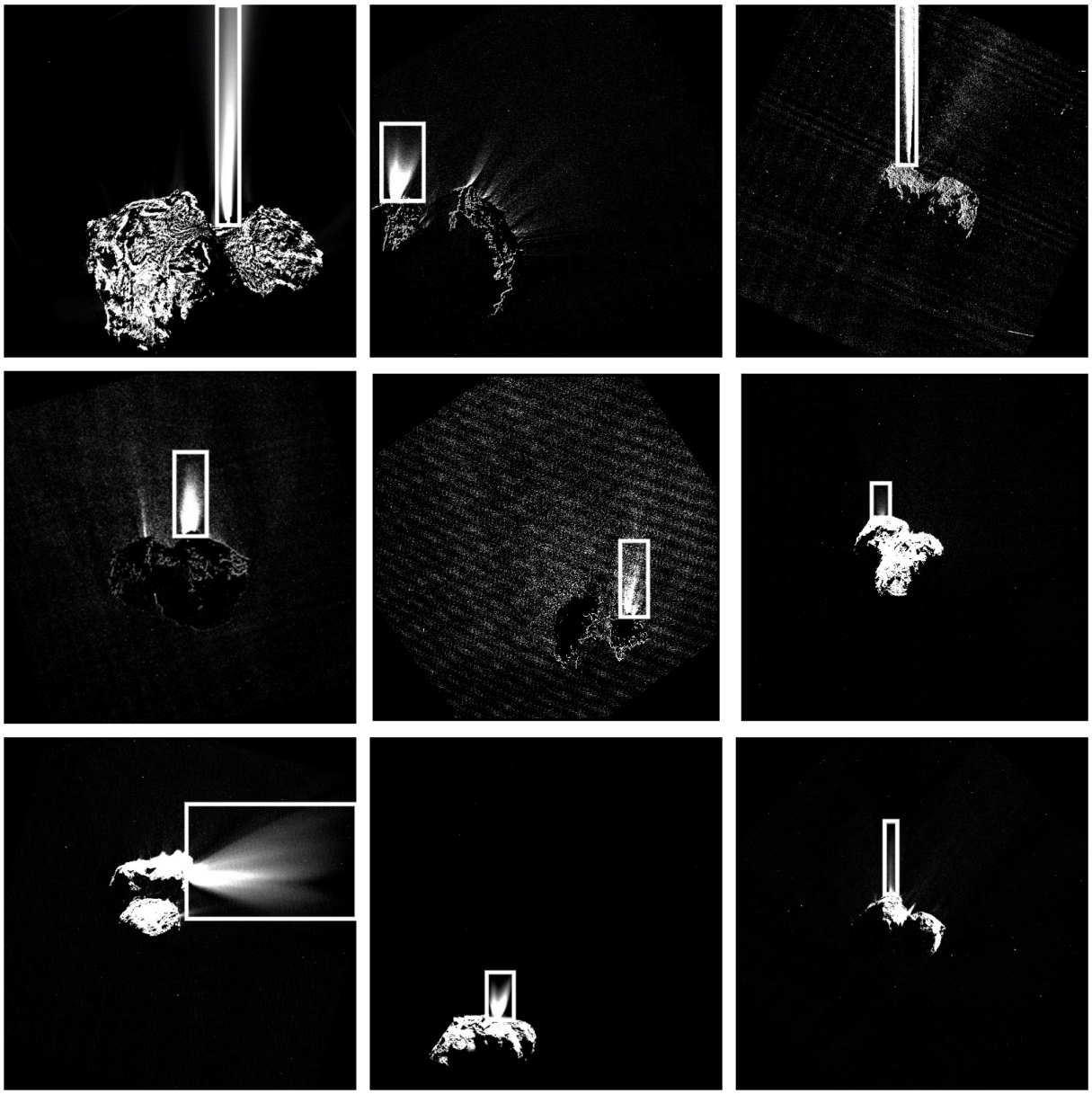

Figure 7. The determined cross-sections were in the selected box (square box). The outburst plumes captured from the difference images on the date were on 2015 July 29, August 5, August 12, August 16, August 26, August 27, August 28, September 3 and September 5 (from left to right, top to bottom). Notice that the angular width of the outburst plumes might not increase as a function of the radial distance because of the subtraction of the low contrast part of the outburst plumes from the other image. Some faint patterns in the images are caused by a compression artefact.

A'Hearn & Meech 2008). More recently, Skorov et al. (2016) proposed that the deepening of a pre-existing fracture or crack on the surface of comet 67P, containing a super-volatile ice (i.e. CO_2 or CO) in the subsurface could lead to a short-lived outburst with a narrow or collimated-like plume. Other possible outburst mechanisms are discussed in more detail by Vincent et al. (2016a) who concluded that some outbursts detected in the morning of cometary local time might be triggered by thermal stresses linked to a rapid change in temperature. Others, occurring in the afternoon, are most likely related to the diurnal or seasonal heat wave reaching volatiles buried deep in the nucleus, while a few of them might be associated with the collapse of a cliff (Pajola et al. 2017).

Additionally, the size distribution of the dust grains might change case-by-case, and vary among the outburst plumes, instead of having the same size distribution for all outbursts. To obtain a precise size distribution, we have to work out which mechanism it is that drives the outbursts, because different mechanisms are proposed regarding the source of the different driving forces that can carry away the different sizes of particles from the cometary surface. The differences in particle size might be related to several different types of outburst morphologies and associated with the investigation of the brightness slopes.

However, regardless of which mechanism is dominant (with the exception of dry outbursts caused by the cliff collapses), the exposed fresh water ice immediately turns to gas, dragging with it the surrounding dust to produce the short-lived collimated jets or debris clouds after the start of the outburst. Furthermore, the ejected mass, which is only a few per cent of the steady-state value of the

Table 2. A summary table of measurements. Mass ejection rates are lower limits assuming that the outburst occurred at a constant rate between two consecutive images. The time interval is measured from two consecutive images.

Start time (UT)	Cross-section (m^2)	Total mass (1 μm to 1 mm) (kg)	Mass ejection rates (kg s^{-1})	Time interval (s)
2015-07-29 13:24:10.760	20234.0	4550.0	4.21/15.16[a]	1080/300[a]
2015-08-05 07:10:32.077	82.4	2.0	0.29	6.29
2015-08-05 08:03:57.736	1917.3	41.7	3.79	11.01
2015-08-12 17:20:36.436	269008.6	5857.5	19.52	300
2015-08-16 22:53:06.769	1287.5	28.0	2.79	10.05
2015-08-26 08:19:55.322	509.1	11.1	1.15	9.6
2015-08-27 03:12:06.804	396.3	8.6	0.74	11.68
2015-08-28 10:09:51.784	26712.9	1270.7	93.30	13.62
2015-09-03 17:57:22.781	654.9	14.3	1.19	12.02
2015-09-03 18:02:22.782	8253.1	179.7	14.95	12.13
2015-09-03 18:07:22.801	20854.3	454.1	37.44	12.03
2015-09-03 18:12:22.782	6668.7	145.2	12.07	12.07
2015-09-03 18:17:22.812	6642.9	144.6	11.98	12.07
2015-09-03 18:22:22.799	1884.1	41.0	3.42	12.01
2015-09-03 18:27:22.764	725.4	15.8	1.31	12.02
2015-09-03 18:32:22.856	654.6	14.3	1.18	12.11
2015-09-03 18:37:22.857	566.0	12.3	1.02	12.12
2015-09-03 18:42:22.814	401.3	8.7	0.73	12.12
2015-09-03 18:47:22.797	132.7	2.9	0.26	11.06
2015-09-03 18:51:32.792	151.3	61.5	0.30	11.08
2015-09-03 18:22:22.799	1570.0	3.3	2.85	12.01
2015-09-05 08:23:55.782	431.657	9.4	0.85	11.05
2015-09-05 08:58:43.857	204424.0	4451.2	14.84	300
2015-09-08 22:40:38.846	310.432	6.8	0.61	11.12
2015-09-10 20:51:22.797	468.571	10.2	0.85	12.03
2015-09-10 21:11:12.538	383.75	8.4	0.81	10.27
2015-09-10 21:11:12.538	28.2102	0.6	0.06	10.27
2015-09-12 09:41:53.733	38359	835.2	2.78	300
2015-09-12 09:46:53.760	43901.7	955.9	3.19	300
2015-09-12 09:51:53.715	119808	2608.7	8.69	300
2015-09-12 09:56:53.734	43040.5	973.2	3.12	300
2015-09-23 21:59:37.739	652.382	14.2	1.29	10.99
2015-09-24 22:56:47.769	48.5774	1.1	0.08	13.0
2015-09-24 23:31:46.762	220.441	4.8	0.47	10.23
2015-09-25 04:18:13.134	4727.39	102.9	10.68	9.64
2015-09-25 05:48:13.288	1262.81	27.5	2.86	9.629
2015-09-25 09:09:39.809	3916.96	85.3	6.55	13.01
2015-09-25 09:14:38.751	2587.71	56.3	5.51	10.2
2015-09-25 09:54:38.764	315.871	6.9	0.58	11.92
2015-09-25 10:39:39.757	186.713	4.1	0.31	12.96
2015-09-25 10:54:38.831	326.525	7.1	0.59	12.06
2015-09-30 11:36:45.774	652.942	14.2	2.67	11.04
2015-09-30 21:34:37.765	921.168	20.1	1.82	11.02
2015-09-30 23:29:55.513	1050.73	22.9	2.13	10.76

Note. [a]We assume that this outburst lasted for a time interval of 300 s.

dust coma, is not comparable to that in some other comets (e.g. 17P/Holmes, 29P/Schwassmann–Wachmann 1). The asymmetric shell of radially expanding material and the features of the outburst plume can be difficult to observe at the time of the outburst. It can be difficult to determine their precise position in enhanced images obtained by ground-based telescopes. It should be possible to obtain a better understanding of the outburst plume dynamics by simulating different kinds of outburst phenomena in the future.

5 SUMMARY

The measurements of outbursts were based on the outburst sequences scheduled by single-filter observations (UV375 filter in the WAC or orange filter in the NAC) and pairs of consecutive images obtained in a short time interval with the NAC orange filter. The main results from the analysis of the images of outbursts in the period 2015 July 29 to September 30 can be summarized as follows. The calculated excess brightness from these outburst plume ranges from a few per cent to ∼28 per cent. In some major outbursts, the brightness contributed by the outburst plume can be one or two times larger than the typical coma jet activities. The strongest outburst is the perihelion outburst detected just a few hours before the comet reaches perihelion. The brightness slopes of the outburst plumes are studied. Some of the detected transient events are interpreted as continuous streams of outflowing gas and dust triggered by driving mechanisms, as yet not understood, which remain active for several

minutes to less than a few hours. The mass ejection rate during a large outburst can reach a few per cent of the steady-state value of the dust coma.

ACKNOWLEDGEMENTS

OSIRIS was built by a consortium led by the Max-Planck-Institut für Sonnensystemforschung, Göttingen, Germany, in collaboration with: CISAS, University of Padova, Italy; the Laboratoire d'Astrophysique de Marseille, France; the Instituto de Astrofísica de Andalucía, CSIC, Granada, Spain; the Scientific Support Office of the European Space Agency, Noordwijk, the Netherlands; the Instituto Nacional de Técnica Aeroespacial, Madrid, Spain; the Universidad Politéchnica de Madrid, Spain; the Department of Physics and Astronomy of Uppsala University, Sweden; and the Institut für Datentechnik und Kommunikationsnetze der Technischen Universität Braunschweig, Germany. The support of the national funding agencies of Germany (Deutschen Zentrums für Luft- und Raumfahrt), France (Centre National d'Etudes Spatales), Italy (Agenzia Spaziale Italiana), Spain (Ministerio de Educación, Cultura y Deporte), Sweden (Swedish National Space Board; grant no. 74/10:2) and the ESA Technical Directorate is gratefully acknowledged. This work was also supported by grant number MOST 105-2112-M-008-002-MY3 from the Ministry of Science and Technology of Taiwan. We are indebted to the whole *Rosetta* mission team, Science Ground Segment, and *Rosetta* Mission Operation Control for their hard work in making this mission possible.

REFERENCES

A'Hearn M. F. et al., 2011, Science, 332, 1396
Bruck Syal M., Schultz P. H., Sunshine J. M., A'Hearn M. F., Farnham T. L., Dearborn D. S. P., 2013, Icarus, 222, 610
Farnham T. L. et al., 2007, Icarus, 187, 26
Farnham T. L., Bodewits D., Li J-Y., Veverka J., Thomas P., Belton M. J. S., 2013, Icarus, 222, 540
Feldman P. D. et al., 2016, ApJ, 825, L8
Fornasier S. et al., 2015, A&A, 583, A30
Fougere N. et al., 2016, MNRAS, 462, 156
Fulle M. et al., 2015, ApJ, 802, 12
Fulle M. et al., 2016, ApJ, 821, 19
Gicquel A. et al., 2016, Earth Moon and Planets, 462, S57
Grün E. et al., 2016, MNRAS, 462, S220
Hansen K. C. et al., 2016, MNRAS, 462, S491
Ipatov S. I., A'Hearn M. F., 2011, MNRAS, 414, 76
Knollenberg J. et al., 2016, A&A, 596, A89
Kolokolova L., Kimura H., 2010, Earth, Planets, and Space, 62, 17
Lara L. et al., 2015, A&A, 583, A9
Lin Z.-Y. et al., 2015, A&A, 583, A11
Lin Z.-Y. et al., 2016, A&A, 588, L3
Pajola M. et al., 2017, Nature Astronomy, 1, 0092
Prialnik D., Bar-Nun A., Podolak M., 1987, ApJ, 319, 993
Prialnik D., A'Hearn M. F., Meech K. J., 2008, MNRAS, 388, L20
Rotundi A. et al., 2015, Science, 347, aaa3905
Schulz R. et al., 2015, Nature, 518, 216
Shi X. et al., 2016, A&A, 586, A7
Sierks H. et al., 2015, Science, 347, aaa1044
Skorov Y. V., Rezac L., Hartogh P., Bazilevsky A. T., Keller H. U., 2016, A&A, 593, A76
Smoluchowski R., 1981, Icarus, 47, 312
Sunshine J. M. et al., 2006, Science, 311, 1453
Vincent J.-B. et al., 2016a, MNRAS, 462, S184
Vincent J.-B. et al., 2016b, A&A, 587, A14

[1]*Institute of Astronomy, National Central University, Chung-Li 32054, Taiwan*
[2]*Deutsches Zentrum für Luft- und Raumfahrt (DLR), Institut für Planetenforschung, Rutherfordstrasse 2, D-12489 Berlin, Germany*
[3]*Department for Astronomy, University of Maryland, College Park, MD 20742-2421, USA*
[4]*Space Science Institute, Macau University of Science and Technology, Macau*
[5]*Institute of Space Sciences, National Central University, Chung-Li 32054, Taiwan*
[6]*Max-Planck Institut für Sonnensystemforschung, Justus-von-Liebig-Weg, 3, D-37077 Göttingen, Germany*
[7]*Department of Physics and Astronomy 'G. Galilei', University of Padova, Vic. Osservatorio 3, I-35122 Padova, Italy*
[8]*Centro di Ateneo di Studi ed Attivitá Spaziali 'Giuseppe Colombo', University of Padova, Via Venezia 15, I-35131 Padova, Italy*
[9]*Laboratoire d'Astrophysique de Marseille, UMR 7326 CNRS and Aix-Marseille Université, 38 rue Frédéric Joliot-Curie, F-13388 Marseille cedex 13, France*
[10]*Centro de Astrobiologia (INTA-CSIC), ESA, ESAC, PO Box 78, E-28691 Villanueva de la Cañada, Madrid, Spain*
[11]*International Space Science Institute, Hallerstrasse 6, CH-3012 Bern, Switzerland*
[12]*Research and Scientific Support Department, European Space Agency, NL-2201 Noordwijk, the Netherlands*
[13]*PAS Space Reserch Center, Bartycka 18A, PL-00716 Warszawa, Poland*
[14]*Institut für Geophysik und extraterrestrische Physik (IGEP), Technische Universität Braunschweig, D-38106 Braunschweig, Germany*
[15]*LESIA-Observatoire de Paris, CNRS, UPMC Univ Paris 06, Univ. Paris-Diderot, 5 Place J. Janssen, 92195 Meudon Pricipal Cedex, France*
[16]*LATMOS, CNRS/UVSQ/IPSL, 11 Boulevard dAlembert, F-78280 Guyancourt, France*
[17]*INAF Osservatorio Astronomico di Padova, Vic. dell'Osservatorio 5, I-35122 Padova, Italy*
[18]*CNR-IFN UOS Padova LUXOR, via Trasea 7, 35131 Padova, Italy*
[19]*Department of Physics and Astronomy, Uppsala University, Box 516, SE-75120 Uppsala, Sweden*
[20]*Department of Industrial Engineering, University of Padova, Via Venezia 1, I-35131 Padova, Italy*
[21]*University of Trento, via Sommarive 9, 38123 Trento, Italy*
[22]*INAF – Osservatorio Astronomico di Trieste, via Tiepolo 11, 34143 Trieste, Italy*
[23]*Instituto de Astrofísica de Andalucía (CSIC), c/Glorieta de la Astronomía, E-18008 Granada, Spain*
[24]*Department of Earth Science, National Central University, Chung-Li 32054, Taiwan*
[25]*Department of Information Engineering, University of Padova, via Gradenigo 6/B, I-35131 Padova, Italy*
[26]*University of Oldenburg, Ammerländer Heerstrabe 114, D-26111 Oldenburg, Germany*
[27]*Physikalisches Institut der Universität Bern, Sidlerstr. 5, CH-3012 Bern, Switzerland*

This paper has been typeset from a TEX/LATEX file prepared by the author.